university of groningen

University Medical Center Groningen

University of Groningen

Highly Selective Hydrogenation of Levulinic Acid to gamma-Valerolactone Over Ru/ZrO2 Catalysts

Filiz, Bilge Coskuner; Gnanakumar, Edwin S.; Martinez-Arias, Arturo; Gengler, Regis; Rudolf, Petra; Rothenberg, Gadi; Shiju, N. Raveendran

Published in:
Catalysis Letters

DOI:
10.1007/s10562-017-2049-x

IMPORTANT NOTE: You are advised to consult the publisher's version (publisher's PDF) if you wish to cite from it. Please check the document version below.

Document Version
Publisher's PDF, also known as Version of record

Publication date:
2017

Link to publication in University of Groningen/UMCG research database

Citation for published version (APA):
Filiz, B. C., Gnanakumar, E. S., Martinez-Arias, A., Gengler, R., Rudolf, P., Rothenberg, G., & Shiju, N. R. (2017). Highly Selective Hydrogenation of Levulinic Acid to gamma-Valerolactone Over Ru/ZrO2 Catalysts. *Catalysis Letters*, *147*(7), 1744-1753. https://doi.org/10.1007/s10562-017-2049-x

Copyright
Other than for strictly personal use, it is not permitted to download or to forward/distribute the text or part of it without the consent of the author(s) and/or copyright holder(s), unless the work is under an open content license (like Creative Commons).

The publication may also be distributed here under the terms of Article 25fa of the Dutch Copyright Act, indicated by the “Taverne” license. More information can be found on the University of Groningen website: https://www.rug.nl/library/open-access/self-archiving-pure/taverne-amendment.

Take-down policy
If you believe that this document breaches copyright please contact us providing details, and we will remove access to the work immediately and investigate your claim.

Downloaded from the University of Groningen/UMCG research database (Pure): http://www.rug.nl/research/portal. For technical reasons the number of authors shown on this cover page is limited to 10 maximum.

Catal Lett (2017) 147:1744–1753
DOI 10.1007/s10562-017-2049-x

Highly Selective Hydrogenation of Levulinic Acid to γ-Valerolactone Over Ru/ZrO_2 Catalysts

Bilge Coşkuner Filiz[1] · Edwin S. Gnanakumar[1] · Arturo Martínez-Arias[2] · Régis Gengler[3] · Petra Rudolf[3] · Gadi Rothenberg[1] · N. Raveendran Shiju[1]

Received: 2 June 2016 / Accepted: 2 April 2017 / Published online: 24 May 2017
© The Author(s) 2017. This article is an open access publication

Abstract We studied the catalytic hydrogenation of levulinic acid over zirconia supported ruthenium catalysts. Four different Ru/ZrO_2 catalysts were prepared by different pre-treatments and using different zirconium supports ($ZrO_x(OH)_{4-2x}$ and ZrO_2). Although the final compositions of the catalysts are the same, the pre-treatments strongly affect catalytic activity. Remarkably, one of the catalysts gave >99% yield of γ-valerolactone under mild conditions. This catalyst was also robust, and could be recycled at least four times without any loss in activity or selectivity. The activity is attributed to the presence of small ruthenium particles together with acidic sites on the catalyst.

Graphical Abstract Pre-treatment changes the performance for ruthenium nanoparticles on zirconia supports, giving TONs over 3500 in the hydrogenation of levulinic acid to γ-valerolactone with over 99% yield.

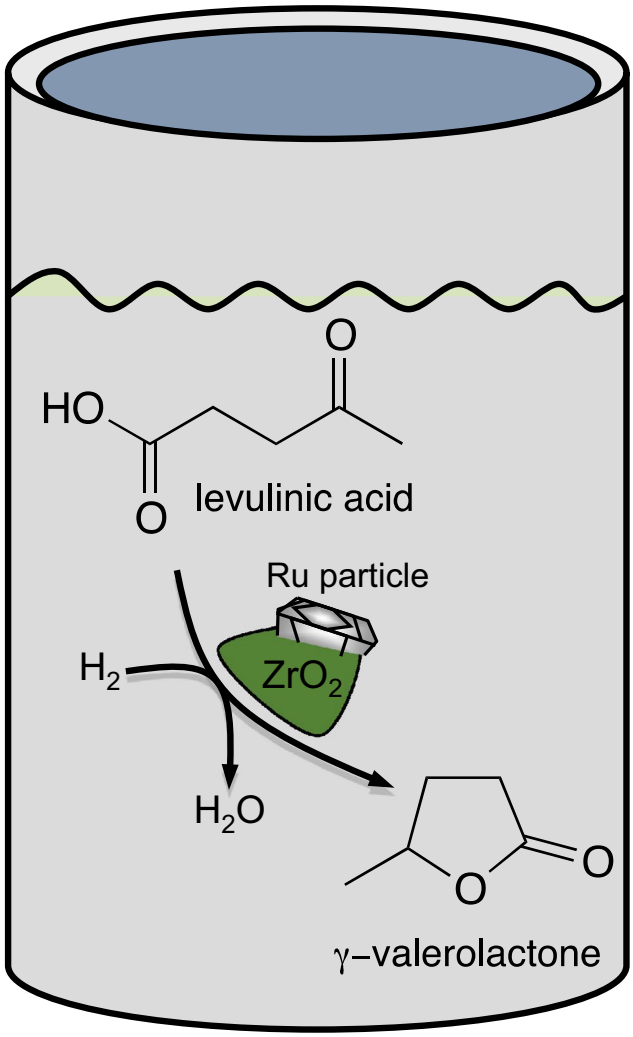

Electronic supplementary material The online version of this article (doi:10.1007/s10562-017-2049-x) contains supplementary material, which is available to authorized users.

✉ N. Raveendran Shiju
n.r.shiju@uva.nl

[1] Van't Hoff Institute for Molecular Sciences, University of Amsterdam, P.O. Box 94157, 1090GD Amsterdam, The Netherlands

[2] Instituto de Catálisis y Petroleoquímica. CSIC, C/ Marie Curie 2. Campus de Cantoblanco, 28049 Madrid, Spain

[3] Zernike Institute for Advanced Materials, University of Groningen, Nijenborgh 4, 9747 AG Groningen, The Netherlands

Keywords γ-Valerolactone · Zirconia · Hydrogenation · Levulinic acid · Biomass conversion · Ruthenium

1 Introduction

Converting lignocellulosic biomass to high-value-added chemicals is a 'hot topic', and rightly so. Biomass is our only practical source of renewable carbon,[1] yet there is enough of it to meet the worldwide demand for polymers, agrochemicals and fine chemicals. But notwithstanding the advantages of its rich chemical variety, practical applications of biomass must focus on a few simple and common building blocks [2–4]. These so-called 'platform molecules' can then be incorporated into existing processes or form the basis for new processes using current unit operations [5–9].

Levulinic acid (LA, **1**) is one of the most promising candidates. It is produced easily and economically from biomass, [10–15] and can be converted into many valuable chemicals. These include γ-valerolactone (GVL, **2**), 1,4-pentanediol, methyltetrahydrofuran, and valeric acid and esters [16, 17]. Of these, the stable and non-toxic GVL has already several applications: it can be used directly as a fuel additive or as a precursor for fuels and chemicals and as a renewable solvent [10, 18–21]. Various companies such as Green Future SRL, DuPont, Segetis and Biofine have developed processes for the manufacturing of levulinic acid through bio-based routes. These processes are expected to reduce the price of levulinic acid from its current US$ 5–8/kg to less than US$ 1/kg [22].

Although the hydrogenation of levulinic acid to GVL was also reported using homogeneous catalysts, any large-scale process is much more likely to use heterogeneous catalysis, owing to the ease of catalyst separation and the simpler product workup [22–24]. The separation costs are often the deciding factor, because any remaining catalyst will often react further with the product and by-products. Supported ruthenium catalysts are known to perform well in LA hydrogenation [10, 19, 25–29]. The problem is that small changes in any number of parameters often cause large variance in catalyst performance. Using different supports and even using different phases of the same compound [30–32] alters conversion and yield [17]. Another parameter that influences catalyst performance is the metal dispersion on the surface. In general, smaller Ru particles are more active, but the catalyst is less robust [17, 19, 31, 33]. Also, it is reported in literature that mixing acid catalysts with Ru metal catalysts promoted hydrogenation and bifunctional catalysts are active and recyclable in aqueous solution [18, 34]. The nature of the support and the synthesis method influence the catalytic activity significantly in hydrogenation reactions [35]. Considering the relatively high cost and low availability of ruthenium, catalyst robustness is a key issue for any practical application [36].

Addressing these challenges, we synthesised several zirconia-supported Ru catalysts and tested these in the liquid phase hydrogenation of LA. We chose zirconia as the support because previous works showed that, for other reactions, its interaction with the active phase enhances activity and selectivity [37, 38]. Moreover, it is more robust than Al_2O_3 and SiO_2, a crucial practical criterion of special importance for biomass derivatives, which are generally reacted under aqueous-phase conditions. Thus the support should withstand the hydrolytic attack and not lose surface area. The surface parameters of zirconia can be tuned by appropriate pre-treatment. For example, the acidity in tungstated zirconia changes significantly depending on whether the calcination is done before or after the impregnation with tungstate groups [39]. Doping zirconium oxide (or hydroxide) can change its surface area, conductivity and crystal structure, affecting the catalytic performance. Again, these parameters depend on the treatment conditions. Here, we found that the pre-treatment strongly influences the hydrogenation results. The best catalyst achieved a turnover number (TON) of 3500, better than any of the values reported so far under similar conditions. This catalyst retained 100% of its activity in four consecutive runs.

2 Experimental Section

2.1 Materials and Instrumentation

Ruthenium chloride ($RuCl_3$), zirconyl chloride octahydrate ($ZrOCl_2$•8H2O, 98%; used as the source of zirconium for preparing the homemade zirconia samples) and DMSO were purchased from Aldrich. Commercial zirconia (TOSOH TZ-3Y) was purchased from Tosoh. Ammonium hydroxide (NH_4OH) and ethyl lactate (98%) were purchased from Fluka. Levulinic acid (LA, 98+%) and ammonium nitrate (NH_4NO_3) were purchased from Acros Organics and Merck, respectively.

Powder X-ray diffraction (XRD) patterns were collected on a Rigaku Mini Flex II diffractometer operating at 15 mA and 30 kV, using Ni-filtered CuKα radiation (λ = 1.5406 Å) with a step size of 0.05°. Temperature programmed reduction (TPR) analyses were carried out on a Thermo Electron TPDRO series 1100 instrument. Samples were pre-treated in N2 (40 cm^3 min^{-1}) at 200 °C for 5 min with 5 °C min^{-1} heating rate before H_2-TPR analyses. Analyses were carried out at a heating rate of 10 °C min^{-1} in 5% H_2/N_2 at a constant flow rate of 20 cm^3 min^{-1}. The N_2 adsorption isotherms were measured at 77 K on a Thermo Scientific Surfer instrument after evacuation at 473 K for 16 h. Surface areas were calculated using the BET method. High

resolution transmission electron microscopy images were acquired with a TEM/STEM JEOL 2100F microscopy operating at 200 kV and with a field emission gun, able to achieve point resolution of 0.19 nm. The microscope is coupled with an EDX detector (INCA x-sight from Oxford Instruments), which allows semi-quantitative chemical analysis of the samples. Specimens were prepared by were prepared by depositing them from ethanol dispersion onto a nickel grid supporting a perforated carbon film. X-ray Photoelectron spectroscopy was performed using a SSX-100 surface science instrument equipped with a monochromatic Al Kα X-ray source (1486.3 eV) with a spot size on the sample of 600 µm. The base pressure during the measurements was 5×10^{-10} mbar. The samples were prepared by drop casting an ethanol dispersion onto gold on mica and dried under vacuum before introduction into the spectrometer. An electron flood gun in combination with a Molybdenum grid placed above the sample was used during measurements to minimize charging effects. The surface ratios of Ru to Zr were calculated from the intensity ratios of the Ru 3d and Zr 3d peaks. Gas chromatography (GC) analyses were performed on a GC8000 Top Interscience chromatograph equipped with a flame ionization detector and a 30 m RTX-1701 column (0.25 mm ID, 1 µm df). Products were identified using standard solutions, and quantified using ethyl lactate as standard. The catalytic tests were carried out in a 35 ml cylindrical stainless steel autoclave, equipped with a PTFE insert and a thermocouple. NH_3-TPD experiments were measured on a Micromeritics AutoChem II 2920 instrument. Approximately 100 mg of sample was initially pretreated at 250 °C under 10% H_2/He (samples A, B and D) or He (sample C) for 30 min and subsequently saturated with 50 ml/min 5% NH_3/He at 40 °C for 60 min. Loosely bound ammonia was hereafter removed by purging with 50 ml/min He for 60 min, before performing temperature programmed desorption (TPD) at a heating rate of 10 °C/min in the range 40–900 °C in a He flow of 25 ml/min.

2.2 Procedure for Preparing Zirconia-supported Ruthenium Catalysts

Zirconium oxohydroxide was prepared by controlled addition of an aqueous zirconium oxychloride ($ZrOCl_2.8H_2O$) solution to an NH_4OH (0.1 M)/NH_4NO_3 (0.1 M) buffer solution, keeping a constant pH 10. The precipitate was filtered under vacuum and washed with deionized water until the filtrate reached pH 7. The solid (zirconium oxyhydroxide, $ZrO_x(OH)_{4-2x}$; denoted hereafter as ZrOH) was filtered and dried at 120 °C for 12 h. ZrO_2 was obtained from this ZrOH after calcination in static air at 500 °C for 4 h .

The four zirconia-supported Ru catalysts **A–D** (5 wt% Ru in all cases) were prepared using different zirconia supports and thermal treatment procedures (see Table 1 for details). The $RuCl_3$ precursor (2.6 mmol) was dissolved in deionized water (50 ml) and heated to 80 °C. Then, 5.0 g of zirconia support (ZrOH or ZrO_2) was added under stirring. The water was evaporated and the cake was dried at 120 °C for 12 h. Thereafter, each sample was subjected to different thermal treatments: Catalyst **A**, prepared using a commercial ZrO_2 support, was calcined in static air at 450 °C for 3 h and then reduced at 250 °C for 2 h (for comparison, a control sample of A was reduced at 350 °C, to check the effect of the reduction temperature on the ruthenium). Catalyst **B**, prepared using a ZrOH support, was calcined in static air at 450 °C for 3 h and then reduced at 250 °C for 2 h. Catalyst **C** was prepared from ZrOH, but first reduced at 250 °C for 2 h and only then calcined (in static air) at 450 °C for 3 h. Finally, catalyst **D** was prepared using the homemade ZrO_2 support, and directly reduced at 250 °C for 2 h. All reduction treatments were carried out under 25 ml/min of H_2:N_2 (1:3 volume ratio) flow in tubular furnace.

2.3 Procedure for Liquid-phase Hydrogenation of Levulinic Acid Over Zirconia-supported Ruthenium Catalyst

In a typical reaction (see Scheme 1, top), the autoclave was loaded with reactant (4.28 mmol), solvent (10 ml), catalyst (either 12.5 or 25 mg) and a stirring bar. It was then purged thrice with N_2 at 296 K, and subsequently pressurized with H_2 (12–27 bar), heated up to the chosen temperature (100, 130 or 170 °C) and kept for desired reaction time (30 min–7 h) while stirring at 750 rpm. The reaction was then quenched by cooling the autoclave rapidly to 25 °C using an ice bath. Then the reaction mixture was centrifuged (3000 rpm; 10 min) and the supernatant was analysed using a GC. The conversion was calculated from the amount of levulinic acid consumed in the

Table 1 Description of catalysts used in this work

Catalyst	Zr source	Support type	Thermal treatment	
A	Tosoh zirconia	ZrO_2	Calcination	Reduction
			450 °C, 3 h	250 °C, 2 h H_2
B	$ZrOCl_2$•$8H_2O$	ZrOH	Calcination	Reduction
			450 °C, 3 h	250 °C, 2 h H_2
C	$ZrOCl_2$•$8H_2O$	ZrOH	Reduction	Calcination
			250 °C, 2 h H_2	450 °C, 3 h
D	$ZrOCl_2$•$8H_2O$	ZrO_2	Reduction	
			250 °C, 2 h H_2	

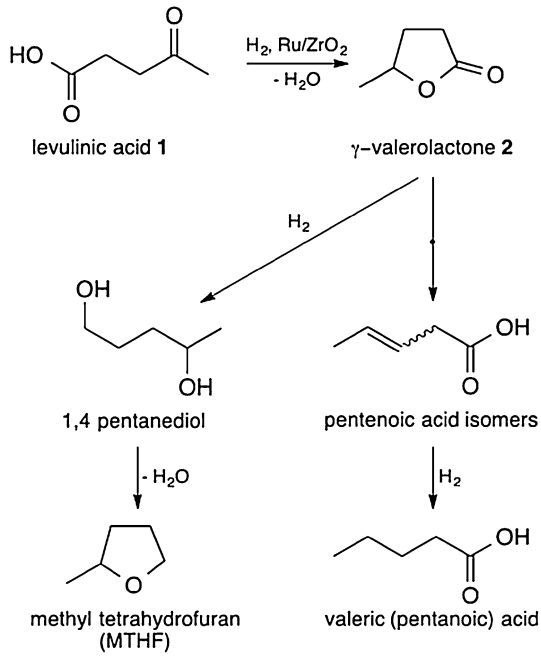

Scheme 1 Catalytic hydrogenation of levulinic acid to various products

reaction. The selectivity was calculated by dividing the amount of GVL formed by the amount of levulinic acid consumed, expressed as percentage. The yield is defined as the product of selectivity and conversion; duplicate analyses confirmed the results, with mass balance >95%. We did not observe any hydrogenation products of GVL by GC. For recycling tests, the catalyst was filtered, washed with acetone, dried at 120 °C for 12 h in air and reduced in 25 ml/min of H_2:N_2 (1:3 volume ratio) flow at 250 °C before the next cycle.

3 Results and Discussion

Converting LA to GVL is not a simple hydrogenation. We must ensure that we hydrogenate only the keto group, enabling the cyclisation to the lactone product. Previous studies have shown that both the size and the dispersion of the ruthenium sites are crucial, as well as the properties of the support [17, 21, 32, 33]. This is because the hydrogenation of keto group is catalysed by a combined effort of both the ruthenium active site and the support. The support activates carbonyl group of LA, while ruthenium efficiently dissociates H_2 [31, 33, 34]. Ruthenium is an excellent hydrogenation catalyst, and ZrO_2 is a known support for hydrogenation, [40–42] dehydration, [43] esterification [38], and isomerization reactions [44–47]. The mechanical, thermal and chemical properties of ZrO_2 are favourable for these reactions. It is stable under coking conditions and remains active even after a week's exposure to hot carboxylic acid [21]. Thus, we chose zirconia as support (ZrOH and ZrO_2) and prepared Ru/ZrO_2 catalysts using different pre-treatments. Such thermal treatments may modify the support properties as well as the ruthenium-support interactions and consequently the catalytic performance.

3.1 Characterization of Zirconia Supported Ru Catalysts

Figure 1 shows the XRD patterns of the supports and Ru/zirconia catalysts. ZrOH gives rise to two broad peaks at around 30° (monoclinic phase) and 52° (tetragonal phase) respectively. ZrO_2, prepared from ZrOH by calcination at 500 °C has both monoclinic and tetragonal phases. However, the monoclinic phase is predominant. Conversely, the majority phase of the commercial TOSOH ZrO_2 is tetragonal (peaks at 2θ ~30°, 35°, 50°, and 60°). For the Ru/ZrO_2 catalysts, the peaks of the ruthenium species could not be observed (expected 2θ values of Ru peaks are 38.3°, 42.1° and 44°, JCPDS No. 06-0663), due to the high dispersion of the particles. Catalyst **A**, prepared by the impregnation of TOSOH ZrO_2, gives rise to a pattern similar to that of the bare support. Catalysts **B** and **C**, despite their different calcination and reductions steps, showed similar crystalline structure (Fig. 1). The monoclinic phase was more dominant in catalyst **D**, prepared by impregnating ZrO_2 followed by reduction [48–50].

The textural properties of supports and Ru/ZrO_2 catalysts are given in Table 2. The commercial TOSOH zirconia was found to have the smallest surface area, 14 m^2 g^{-1}. The ZrOH support, prepared by precipitation from $ZrOCl_2$, has a surface area of 197 m^2 g^{-1}, which decreases to 57 m^2 g^{-1} after calcination to ZrO_2. Nevertheless, catalysts **B** and **C**, prepared from ZrOH, have higher surface areas compared to **A** and **D**, which were prepared from ZrO_2. Note that these samples were synthesized by first impregnating the zirconium hydroxide followed by heat treatment. We observed in a previous study that when zirconium hydroxide is first impregnated with WO_x and then calcined, the decrease in surface area is lower compared to calcination of zirconium hydroxide alone [37]. Our results show a similar behaviour with $RuCl_3$ impregnation, but the effect is not as dominant as that reported for WO_x/ZrO_2.

Figure 2 shows the nitrogen adsorption–desorption isotherms of zirconia supports and Ru/ZrO_2 catalysts. The isotherms of the supports are of different types; commercial TOSOH zirconia gives a Type II isotherm with 48 nm average pore diameter (on the border between meso- and macropores), while ZrOH shows a Type I isotherm, mostly microporous, with a 3.7 nm average pore size. The isotherm changes into Type IV and the average pore size nearly doubles (to 6.5 nm) after calcination to ZrO_2.

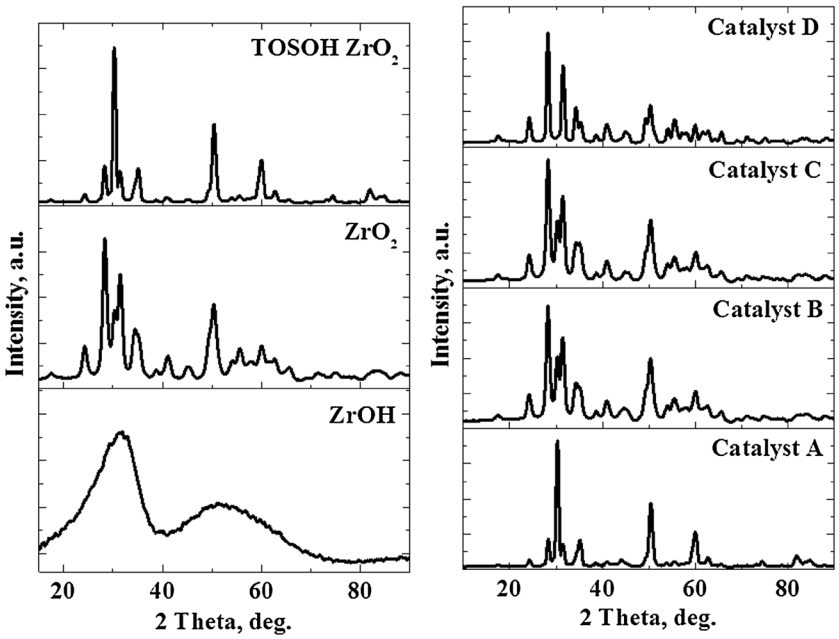

Fig. 1 Powder X-ray diffraction patterns of the supports (*left*) and the four Ru/ZrO_2 catalysts **A**–**D** (*right*)

Table 2 Surface properties of supports and Ru/ZrO_2 catalyst

Material	BET surface area ($m^2\ g^{-1}$)	Specific pore volume ($cm^3\ g^{-1}$)
ZrOH	197	0.16
ZrO_2	57	0.16
TOSOH ZrO_2	14	0.08
A	20	0.30
B	65	0.25
C	63	0.26
D	22	0.09

Impregnating ruthenium on TOSOH zirconia (catalyst **A**), does not change the isotherm dramatically. Catalysts **B, C** and **D** show a classical Type IV (mesoporous) isotherm. The average pore sizes of catalysts B and C, prepared from ZrOH, were similar (5.9 and 6.0 nm, respectively). The average pore size of **D** almost doubles (14.6 nm) after ruthenium impregnation. Note that the surface area and the pore volume decrease while the average pore size increases. This shows that the impregnation and subsequent reduction of ZrO_2 breaks down the original texture. The inner walls collapse, creating fewer (yet larger) pores.

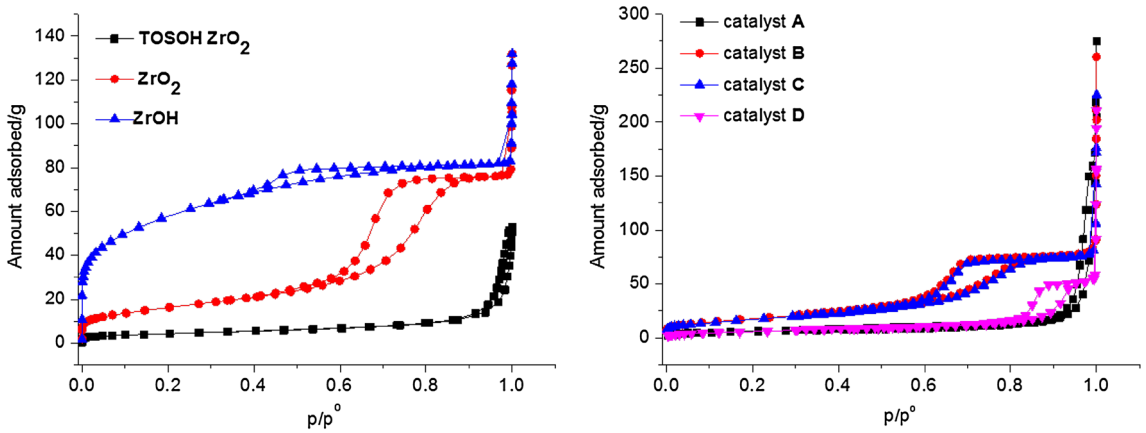

Fig. 2 Adsorption isotherms of supports and Ru/ZrO_2 catalysts

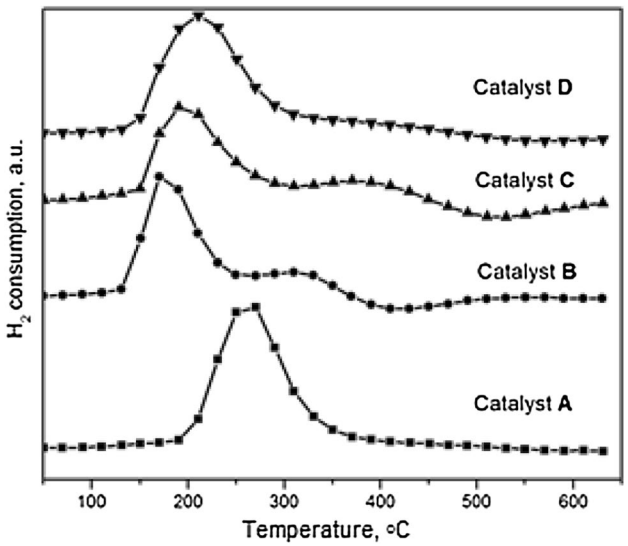

Fig. 3 TPR profiles of the calcined Ru/ZrO_2 catalysts A–D. Conditions: pre-treatment in N_2 (40 cm^3 min^{-1}) at 200 °C for 5 followed by 10 °C min^{-1} in 20 cm^3 min^{-1} of 5% H_2/N_2. Only ca. 30 points are shown per graph for clarity; the actual measurement data contains ca. 300 points per curve

Figure 3 shows the temperature-programmed reduction profiles of the calcined Ru/ZrO_2 catalysts **A–D**. All four catalysts show different reduction behaviour that reflects the different Ru species and interaction forces between the Ru particles and the supports [51–54]. Control experiments confirmed that the bare support shows only a very small reduction peak at ca. 240 °C (data not shown).

We assume that the peaks at 175–250 °C correspond to the reduction of well-dispersed RuO_x species. The higher reduction temperatures indicate a strong metal–support interaction. Catalyst **A** shows only one peak, with a maximum around 250 °C, indicating that the Ru particles are uniformly dispersed. Catalyst **D** also shows one peak with slightly lower maximum. Catalysts **B** and **C** show a minor peak besides the main peak, indicating the presence of a minor species with strong support interaction. These samples also have higher surface area than the rest (around 60 m^2 g^{-1} as compared to 20 m^2 g^{-1} of catalysts **A** and **D**), which might help in dispersing the RuO_x species.

Information on morphological aspects was obtained by the direct low magnification TEM images of the samples. All samples are basically agglomerates of more or less rounded nanoparticles, with relatively larger size for **A** and **D** compared to **B** and **C**. Note that **B** and **C** are prepared by the calcination of ZrOH after loading $RuCl_3$ while **A** and **D** were prepared by loading $RuCl_3$ on pre-calcined ZrOH. The results are analogous to the ones we reported elsewhere for WO_x/ZrO_2 catalysts,[17] where the calcination of WO_x doped ZrOH yielded smaller nanoparticles compared to the calcined, undoped ZrOH. More insight is obtained from a detailed analysis of selected representative high resolution images (see Fig. 4). For **D**, the presence of small ruthenium particles (interplanar distance of ca. 2.06 Å, corresponding to (101) planes of metallic ruthenium) supported on zirconia (interplanar distance of ca. 3.15 Å, related to ($\bar{1}$11) planes of monoclinic zirconia) in profile as well as front view can be identified. This agrees with the XRD pattern, which also showed the predominant formation of the monoclinic phase. The Ru particles appear as truncated semicubooctahedral shapes. They are of around 3–4 nm long and 1–2 nm high.

Sample **A** is similar, although the ruthenium particles appear smaller and more difficult to detect in this case. In contrast, supported ruthenium particles could not be identified in the high resolution images of samples **B** and **C**, suggesting that they are highly dispersed. Note that the parallel EDX analysis (not shown here) evidences the presence of ruthenium, and the TPR analysis shows Ru reduction peaks for **B** and **C**, the areas of which are not very different from those in **A** and **D**. The zirconia nanoparticles in **B** and **C** have tetragonal phase (based on the interplanar distance of ca. 2.6 Å related to (002) planes observed in most cases where lattice fringes could be resolved). Previously we observed that doping ZrOH with WO_x followed by calcination leads to predominant formation of tetragonal ZrO_2.[17] The present results show that tetragonal phase stabilization by doping is more general.

3.2 Levulinic Acid Hydrogenation

We then tested our Ru/ZrO_2 catalysts in the hydrogenation of LA in a batch reactor at 130 °C under 12 bar H_2. A blank reaction without catalyst showed no conversion. All four catalysts were 100% selective for GVL but we observed large differences in catalytic activity (Fig. 5). Catalyst **D**, which was prepared from ZrO_2 and directly reduced under H_2 atmosphere, was the most active, despite its low surface area. Indeed, we found no relation between surface area and activity. Catalyst **B**, with a threefold higher surface area than **A**, showed a similar catalytic activity. Moreover, **B** and **C** have similar surface areas, yet **C** is almost twice as active than **B**. In a separate control experiment, we also pre-reduced catalyst A at 350 °C (catalyst **A-350**) to examine the effect of completely reduced ruthenium sites. As Fig. 5 shows, the reduction temperature affects the conversion of LA, yet the reaction does not depend only on the reduction of all ruthenium species. A direct correlation with the surface areas will not be straight forward also because of the bifunctional character of the reaction, with the metal for the hydrogenation of the carbonyl group and the acid support for the cyclizing esterification.

The XRD and TEM studies show that the crystalline phase of ZrO_2 in **B** and **C** is different from **A** and **D**. This

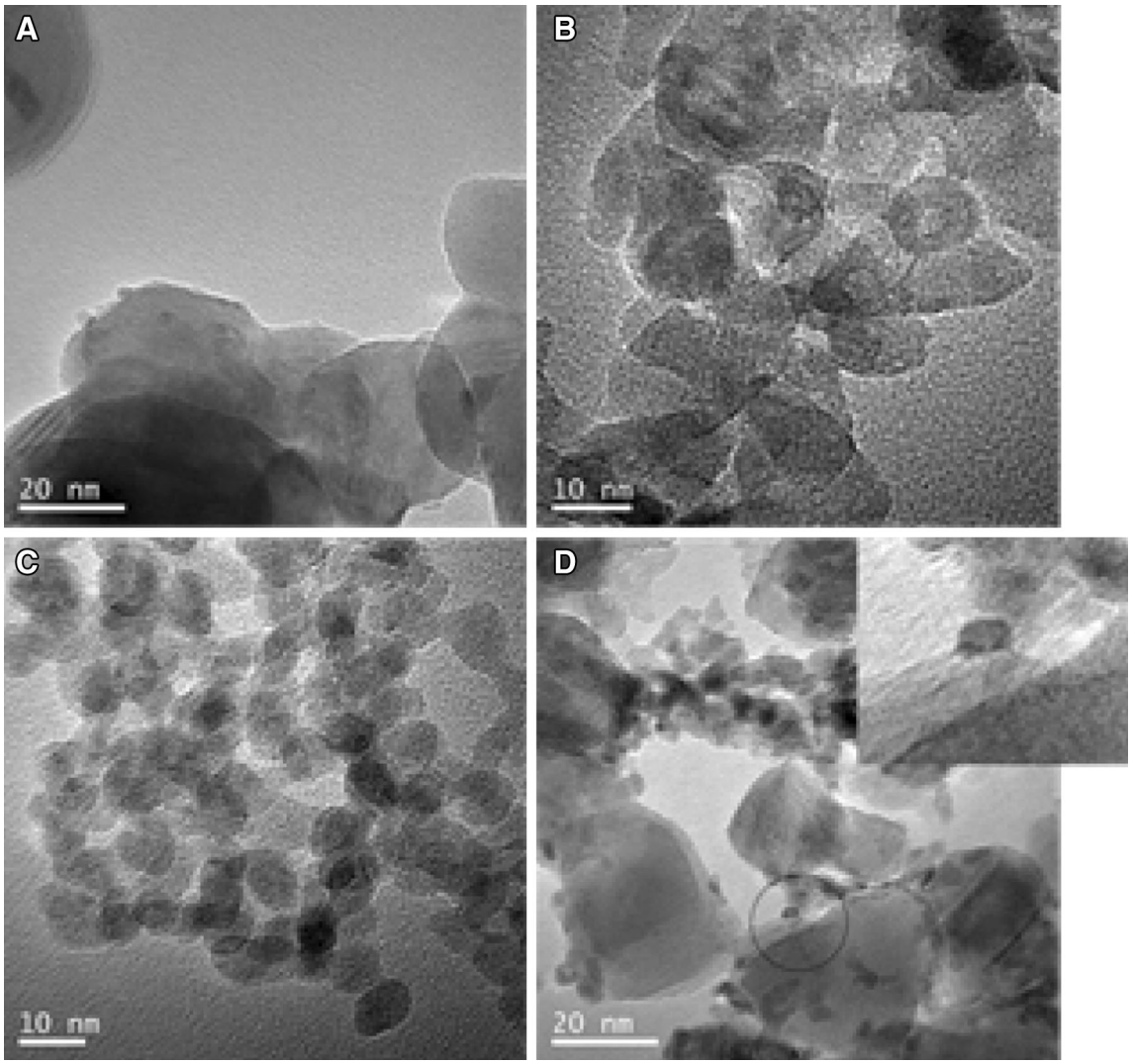

Fig. 4 High resolution TEM images of catalysts **A–D**. The *inset* in image **D** expands the zone enclosed with a circle

could affect the environment of Ru particles. The TEM identifies more or less uniform Ru particles of 3–4 nm in sample **D**, which has the highest catalytic activity. The presence of these well-defined Ru nanoparticles, most of which can be easily reduced as shown by TPR, could account for the high activity of **D**. The assumption, based on TPR, that samples **B** and **C** contain dispersed RuO_x species also agrees with the fact that TEM could not identify the Ru particles on **B** and **C**. Thus the lower activity of **B** and **C** might be attributed to absence of crystalline Ru.

Bulk elemental analysis by ICP-AES did not give any major difference between the samples (5 ± 0.4 wt% Ru). We also analysed the samples by XPS (Catalysts **B** and **D** are shown in Fig. 6). The surface ratios of Ru to Zr obtained from XPS analysis based on the areas of Ru 3d and Zr 3d peaks (after correcting with the instrument specific sensitivity factor) were similar. This means that the surface concentrations of Ru on these catalysts are similar. This in turn means that the comparative lower activity of **B** is not due to Ru being buried in the bulk. Previously, we observed that doping zirconium hydroxide with tungstate groups followed by calcination causes the segregation of WO_3 species at the grain boundaries of zirconia. Contrarily, doping tungstate on pre-formed crystalline ZrO_2 showed no such preference, but resulted in bigger tungstate species and lower catalytic activity [39]. Here we did not observe such differences. Thus, the effect of treatment steps on the final structure of the catalyst depends on the nature of the supported species. We also studied the acidity of the catalysts by NH_3 TPD (Fig. 7), and found that all catalysts have some acidity. An intense peak between 450 and 500 °C for sample **D** shows the presence of strong acid sites, which could be either Brønsted or Lewis in nature. Zirconia is known to possess both Brønsted and Lewis acid

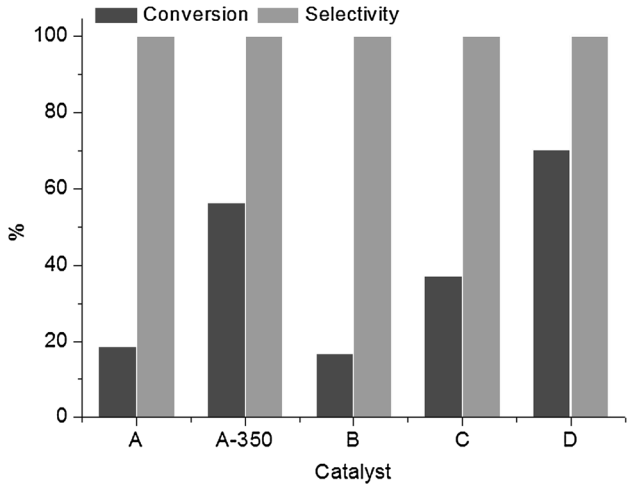

Fig. 5 The activities of Ru/ZrO_2 catalysts for liquid phase hydrogenation of levulinic acid. Reaction conditions: 4.28 mmol LA, 10 ml Water, 25 mg catalyst, 5 wt% Ru catalysts; 0.012 mmol Ru, 130 °C, 12 bar H_2, 120 min

sites and their density depend on pretreatment temperature. The fact that this peak is strongest for **D**, which was synthesized by direct reduction of Ru loaded zirconium oxide (see Table 1), shows that further calcination (as applied in the case of the other samples) diminishes these acid sites. The TPD of bare support did not show any major peaks (Figure S3). The strong peak in TPD of sample D may also originate from remaining small amounts of chloride. Overall, we conclude that the well-defined nanoparticles of Ru together with higher concentration of acid sites make catalyst **D** better than other catalysts.

Since catalyst **D** was the most active, we used it for further reaction optimization studies. The conversion changed with reaction conditions, but the catalyst retained its selectivity to GVL. The conversion as a function of reaction time for this catalyst is provided in supplementary information (Fig. S1).

At 12 bar H_2 pressure, the LA conversion was 70%; increasing the pressure to 24 bar gave complete LA conversion (Table 3, entries 1 and 2) due to the saturation of active catalyst sites by H_2. The effect of the reaction temperature on the conversion of LA was also studied (entries 2 and 3). By decreasing the temperature from 130 to 100 °C, the conversion decreased to 96%. The amount of catalyst also affected the conversion, as expected (entries 2 and 4). Decreased conversion was obtained at shorter reaction times (entries 2 and 5, 6). Under these reaction conditions, full conversion of LA to GVL requires 120 min. We then did the reaction with a higher substrate/catalyst ratio of 2100 (entry 7) full conversion was achieved in 7 h at 170 °C retaining the selectivity to GVL. Under the same conditions, we did an experiment with still higher ratio (3500) but this time replacing H_2O by DMSO as solvent (entry 8). This reaction also gave complete conversion, achieving a TOF of 0.07 s^{-1}, which is higher than the reported values under similar conditions. For example, the TOF values reported previously for various catalysts are 0.03 s^{-1} (5%Ru/C) [17], 0.027 s^{-1} (5%Ru/TiO_2-P25) [17], 0.0059 s^{-1} (5%Ru/TiO_2) [33], 0.0137 (0.6%Ru/TiO_2) [33], 0.002 s^{-1} (5%Pd/C) [32], 0.008 s^{-1} (RuSn/C) [55], 0.00049 s^{-1} (15% RuRe/C) [56], 0.004 s^{-1} (1% Au/TiO_2) [57] and 0.005 s^{-1} (1% Pd/TiO_2) [57].

3.3 Recycling Tests

We re-used catalyst **D** four times (Fig. S2) at low conversion; after each reaction, the catalyst was removed and washed with water and acetone and dried at 120 °C in a static oven. The recycling tests were carried out under the same conditions and we did not see any indication for deactivation. Thus, this Ru/ZrO_2 catalyst is reusable and fully selective to GVL.

Two possible pathways are reported for LA hydrogenation in literature [58]. In the first route, an intramolecular esterification of LA leads to angelica lactones (α and β

Table 3 Activities of catalyst **D** under various conditions

Entry	Catalyst **D** (mg)	T (°C)	P (bar)	t (min)	Conversion (%)	Selectivity (%)
1	25	130	12	120	70	99.9
2	25	130	24	120	99.9	99.9
3	25	100	24	120	95.7	99.9
4	12.5	130	24	120	75	99.9
5	25	130	24	60	66.6	99.9
6	25	130	24	90	96	99.9
7[a]	25	170	27	900	99	99.9
8[b]	25	170	27	900	99	99.9

Reaction conditions: 4.28 mmol LA, 10 ml water, 5 wt% Ru catalyst: 0.012 mmol Ru

[a]25.2 mmol LA, 10 ml water, 5 wt% Ru catalyst: 0.012 mmol Ru

[b]42.8 mmol LA, 10 ml DMSO, 5 wt% Ru catalyst: 0.012 mmol Ru

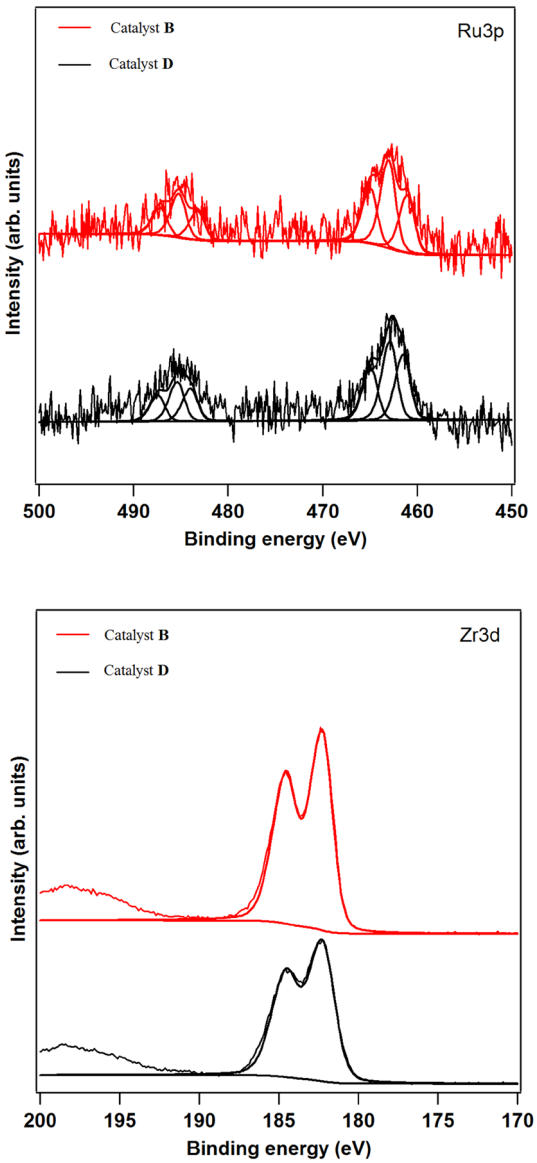

Fig. 6 Ru 3p (*top*) and Zr 3d (*bottom*) XPS spectra of catalysts **B** and **D**. Ru 3d overlaps with C1s spectra and thus not shown

forms) followed by the hydrogenation of the C=C bond. The second pathway involves the hydrogenation of keto groups first, forming 4-hydroxypentanoic acid followed by an intramolecular esterification step. In presence of hydrogen at temperatures higher than 50 °C, the most probable one is the latter [58]. The acidity of the catalyst plays a role in both reaction steps [34]. The second pathway is the more probable one under our conditions (1.2 or 2.4 MPa and 100 or 130 °C).

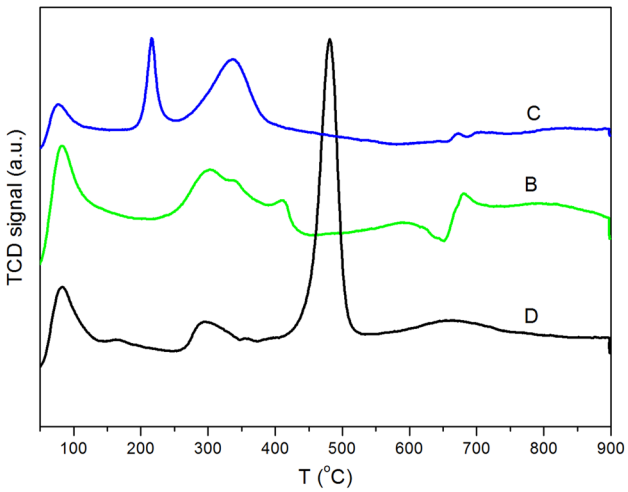

Fig. 7 NH_3 TPD results for samples **B, C** and **D**. An intense peak between 450 and 500 °C in sample **D** shows the presence of strong acid sites

4 Conclusion

We report here a green catalytic route for producing GVL, an important platform molecule in biomass conversion. Our heterogeneous hydrogenation of levulinic acid can be done in water. The catalytic activity is influenced by the pre-treatment conditions. The best catalyst was obtained by the impregnation of $RuCl_3$ on pre-calcined ZrO_2 followed by reduction (catalyst **D**). The Ru particles of 3–4 nm size are uniformly dispersed in this catalyst. This catalyst is highly selective (>99.9%), highly active (>99.9%) and recyclable. The presence of small ruthenium particles together with a higher concentration of acidic sites is responsible for the superior quality of this catalyst.

Acknowledgements We thank N. J. Geels and Dr. M. C. Mittelmeijer-Hazeleger for help with N_2 adsorption measurements, Dr. M. C. Capel and ICP-CSIC Unidad de Apoyo for the TEM and TPD measurements. We also thank NWO CAPITA ERA-NET and COST project (CM1104) for funding parts of the project. This work is part of the Research Priority Area Sustainable Chemistry of the UvA, http://suschem.uva.nl.

Open Access This article is distributed under the terms of the Creative Commons Attribution 4.0 International License (http://creativecommons.org/licenses/by/4.0/), which permits unrestricted use, distribution, and reproduction in any medium, provided you give appropriate credit to the original author(s) and the source, provide a link to the Creative Commons license, and indicate if changes were made.

References

1. Strassberger Z, Tanase S, Rothenberg G (2014) RSC Adv 4:25310–25318
2. Demma Cara P, Ciriminna R, Shiju NR, Rothenberg G, Pagliaro M (2014) ChemSusChem 7:835–840
3. Ramos-Fernandez EV, Geels NJ, Shiju NR, Rothenberg G (2014) Green Chem 16:3358–3363
4. Carlos Serrano-Ruiz J, Dumesic JA (2011) Energy Environ Sci 4:83–99
5. Gallezot P (2012) Chem Soc Rev 41:1538–1558
6. Van de Vyver S, Thomas J, Geboers J, Keyzer S, Smet M, Dehaen W, Jacobs PA, Sels BF (2011) Energy Environ Sci 4:3601–3610
7. Beerthuis R, Granollers M, Brown DR, Salavagione HJ, Rothenberg G, Shiju NR (2015) RSC Adv 5:4103–4108
8. Cara PD, Pagliaro M, Elmekawy A, Brown DR, Verschuren P, Shiju NR, Rothenberg G (2013) Catal Sci Technol 3:2057–2061
9. Caro C, Thirunavukkarasu K, Anilkumar M, Shiju NR, Rothenberg (2012) Adv Synth Catal 354:1327–1336
10. Wright WRH, Palkovits R (2012) ChemSusChem 5:1657–1667
11. Gurbuz EI, Alonso DM, Bond JQ, Dumesic JA (2011) ChemSusChem 4:357–361
12. Corma A, Oliver-Tomas B, Renz M, Simakova IL (2014) J Mol Catal A 388:116–122
13. Demolis A, Essayem N, Rataboul F (2014) ACS Sustain Chem Eng 2:1338–1352
14. Lange JP, van de Graaf WD, Haan RJ (2009) ChemSusChem 2:437–441
15. Hengne AM, Kamble SB, Rode CV (2013) Green Chem 15:2540–2547
16. Luo WH, Deka U, Beale AM, van Eck ERH, Bruijnincx PCA, Weckhuysen BM (2013) J Catal 301:175–186
17. Al-Shaal MG, Wright WRH, Palkovits R (2012) Green Chem 14:1260–1263
18. YaoY, Wang Z, Zhao S, Wang D, Wu Z, Zhang M (2014) Catal Today 234:245–250
19. Yan ZP, Lin L, Liu SJ (2009) Energy Fuels 23:3853–3858
20. Alonso DM, Wettstein SG, Dumesic JA (2013) Green Chem 15:584–595
21. Lange JP, Price R, Ayoub PM, Louis J, Petrus L, Clarke L, Gosselink H (2010) Angew Chem Int Ed 49:4479–4483
22. http://www.grandviewresearch.com/press-release/global-levulinic-acid-market
23. Ras EJ, Rothenberg G (2014) RSC Adv 4:5963–5974
24. Ras EJ, Maisuls S, Haesakkers P, Gruter GJ, Rothenberg G (2009) Adv Synth Catal 351:3175–3185
25. Manzer LE (2004) Appl Catal A 272:249–256
26. Manzer LE (2002) WO Patent 2,002,074,760 A1
27. Tukacs JM, Kiraly D, Stradi A, Novodarszki G, Eke Z, Dibo G, Kegl T, Mika LT (2012) Green Chem 14:2057–2065
28. Wettstein SG, Bond JQ, Alonso DM, Pham HN, Datye AK, Dumesic JA (2012) Appl Catal B 117:321–329
29. Moreno Marrodan C, Barbaro P (2014) Green Chem 16:3434–3438
30. Bourne RA, Stevens JG, Ke J, Poliakoff M (2007) Chem Commun 44:4632–4634
31. Xiao C, Goh TW, Qi Z, Goes S, Brashler K, Perez C, Huang W 2016 ACS Catal 6:593–599
32. Upare PP, Lee JM, Hwang DW, Halligudi SB, Hwang YK, Chang JS (2011) J Ind Eng Chem 17:287–292
33. Primo A, Concepcion P, Corma A (2011) Chem Commun 47:3613–3615
34. Galletti AMR, Antonetti C, De Luise V, Martinelli M (2012) Green Chem 14: 688–694
35. Ruppert AM, Grams J, Jedrzejczyk M, Matras-Michalska J, Keller N, Ostojska K, Sautet P (2015) ChemSusChem 8:1538–1547
36. Hernandez-Mejia C, Gnanakumar ES, Olivos-Suarez A, Gascon J, Greer HF, Zhou WZ, Rothenberg G, Shiju NR (2016) Catal Sci Technol 6:577–582
37. Shiju NR, AnilKumar M, Hoelderich WF, Brown DR (2009) J Phys Chem C 113:7735–7742
38. Grecea ML, Dimian AC, Tanase S, Subbiah V, Rothenberg G (2012) Catal Sci Technol 2:1500–1506
39. Shiju NR, Yoshida K, Boyes ED, Brown R, Gai PL (2011) Catal Sci Technol 1:413–425
40. Ardiyanti AR, Gutierrez A, Honkela ML, Krause AOI, Heeres HJ (2011) Appl. Catal. A 407:56
41. Han J, Kim YH, Jang HS, Hwang SY, Jegal J, Kim JW, Lee YS (2016) RSC Adv 6:93394
42. Hao WW, Li WF, Tang X, Zeng XH, Sun Y, Liu SJ, Lin L (2016) Green Chem 18:1080
43. Ferino I, Casula MF, Corrias A, Cutrufello MG, Monaci R, Paschina G (2000) Phys Chem Chem Phys 2:1847–1854
44. Iglesias J, Melero JA, Morales G, Paniagua M, Hernandez B (2016) ChemCatChem 8:2089
45. Osatiashtiani A, Lee AF, Granollers M, Brown DR, Olivi L, Morales G, Melero JA, Wilson K (2015) ACS Catal 5:4345
46. Suzuki T, Yokoi T, Otomo R, Kondo JN, Tatsumi T (2011) Appl Catal A 408:117
47. Ebitani K, Konishi J, Hattori H (1991) J Catal 130:257–267
48. Sun GL, Xu AH, He Y, Yang M, Du HZ, Sun CL (2008) J Hazard Mater 156:335–341
49. Rezaei M, Alavi SM, Sahebdelfar S, Yan ZF (2006) Powder Technol 168:59–63
50. Gionco C, Paganini MC, Giamello E, Burgess R, Di Valentin C, Pacchioni G (2013) Chem Mater 25:2243–2253
51. Coq B, Kumbhar PS, Moreau C, Moreau P, Figueras F (1994) J Phys Chem 98:10180–10188
52. Sun J, Li XG, Taguchi A, Abe T, Niu WQ, Lu P, Yoneyarna Y, Tsubaki N (2014) ACS Catal 4:1–8
53. Zonetti PD, Landers R, Cobo AJG (2008) Appl Surf Sci 254:6849–6853
54. Lin QQ, Liu XY, Jiang Y, Wang Y, Huang YQ, Zhang T (2014) Catal Sci Technol 4:2058–2063
55. Alonso DM, Wettstein SG, Bond JQ, Root TW, Dumesic JA (2011) ChemSusChem 4:1078–1081
56. Braden DJ, Henao CA, Heltzel J, Maravelias CT, Dumesic JA (2011) Green Chem 13:1755–1765
57. Luo WH, Sankar M, Beale AM, He Q, Kiely CJ, Bruijnincx PCA, Weckhuysen BM (2015) Nat Commun 6:6540
58. Abdelrahman OA, Heyden A, Bond JQ (2014) ACS Catal 4:1171–1181